A Lagrangian Climatology of Tropical Moisture Exports to the Northern Hemispheric Extratropics

PETER KNIPPERTZ* AND HEINI WERNLI[+]

Institute for Atmospheric Physics, Johannes Gutenberg University Mainz, Mainz, Germany

ABSTRACT

Case studies have shown that heavy precipitation events and rapid cyclogenesis in the extratropics can be fueled by moist and warm tropical air masses. Often the tropical moisture export (TME) occurs through a longitudinally confined region in the subtropics. Here a comprehensive climatological analysis of TME is constructed on the basis of seven-day forward trajectories started daily from the tropical lower troposphere using 6-hourly 40-yr ECMWF Re-Analysis (ERA-40) data from the 23-year period 1979–2001. The objective TME identification procedure retains only those trajectories that reach a water vapor flux of at least 100 $g\ kg^{-1}\ m\ s^{-1}$ somewhere north of 35°N. The results show four distinct activity maxima with different seasonal behavior: (i) The ''pineapple express,'' which connects tropical moisture sources near Hawaii with precipitation near the North American west coast, has a marked activity maximum in boreal winter. (ii) TME over the west Pacific is largest in summer, partly related to the East Asian monsoon and the mei-yu–baiu front. This region alone is responsible for a large portion of TME across 35°N. (iii) The narrow activity maximum over the Great Plains of North America is rooted over the Gulf of Mexico and the Caribbean Sea and has a clear maximum in summer and spring. (iv) TME over the western North Atlantic shows the smallest annual cycle with a maximum in winter and autumn. The interannual variability of (i) and (iv) is significantly modulated by El Niño. Over the African–European–Asian region, high orographic barriers impede TME. A typical TME trajectory evolution is poleward and quasi-horizontal in the subtropics and then more eastward and upward in the southern midlatitudes, where TME contributes up to 60% to climatological precipitation. The TME dataset presented here can serve as a basis for future studies on extreme events.

1. Introduction

Horizontal and vertical transports of water vapor in the atmosphere are an important part of the general circulation and crucial for the earth's water and energy budgets (Peixoto and Oort 1992). In a zonally averaged sense, the main source for atmospheric moisture is ocean evaporation in the region of the subsiding branches of the Hadley circulation around 25°N/S. The equatorward parts of the large subtropical maritime highs are located in this region, where evaporation exceeds precipitation by as much as 5 mm day^{-1} (Kållberg et al. 2005). The main transport pathways away from these source regions are into the midlatitude storm tracks (mainly poleward of 30°N/S) and with the trade winds into the intertropical convergence zone (ITCZ; mainly equatorward of 20°N/S). Interestingly, if the zonal circulation is averaged in a quasi-Lagrangian sense on dry or moist isentropes instead of pressure surfaces, the resulting meridional mass streamfunction indicates a direct circulation from the tropics into high latitudes aloft (Walker and Schneider 2006; Pauluis et al. 2008).

Zonal cross sections of the climatological meridional water vapor transport along 35°N illustrate distinct longitudinal and seasonal variations of this general pattern (Fig. 1). The Azores high dominates the subtropical North Atlantic sector during all seasons, resulting in poleward moisture transports between the Rocky Mountains and about 30°W and equatorward transports over the eastern North Atlantic, the Mediterranean region, and parts of Asia, where meridional circulations are hindered by significant orographic barriers. There are

---

* School of Earth and Environment, University of Leeds, Leeds, United Kingdom.
[+] Institute for Atmospheric and Climate Science, ETH Zurich, Zurich, Switzerland.

Corresponding author address: Peter Knippertz, Institute for Climate and Atmospheric Science, School of Earth and Environment, University of Leeds, Leeds LS2 9JT, United Kingdom.
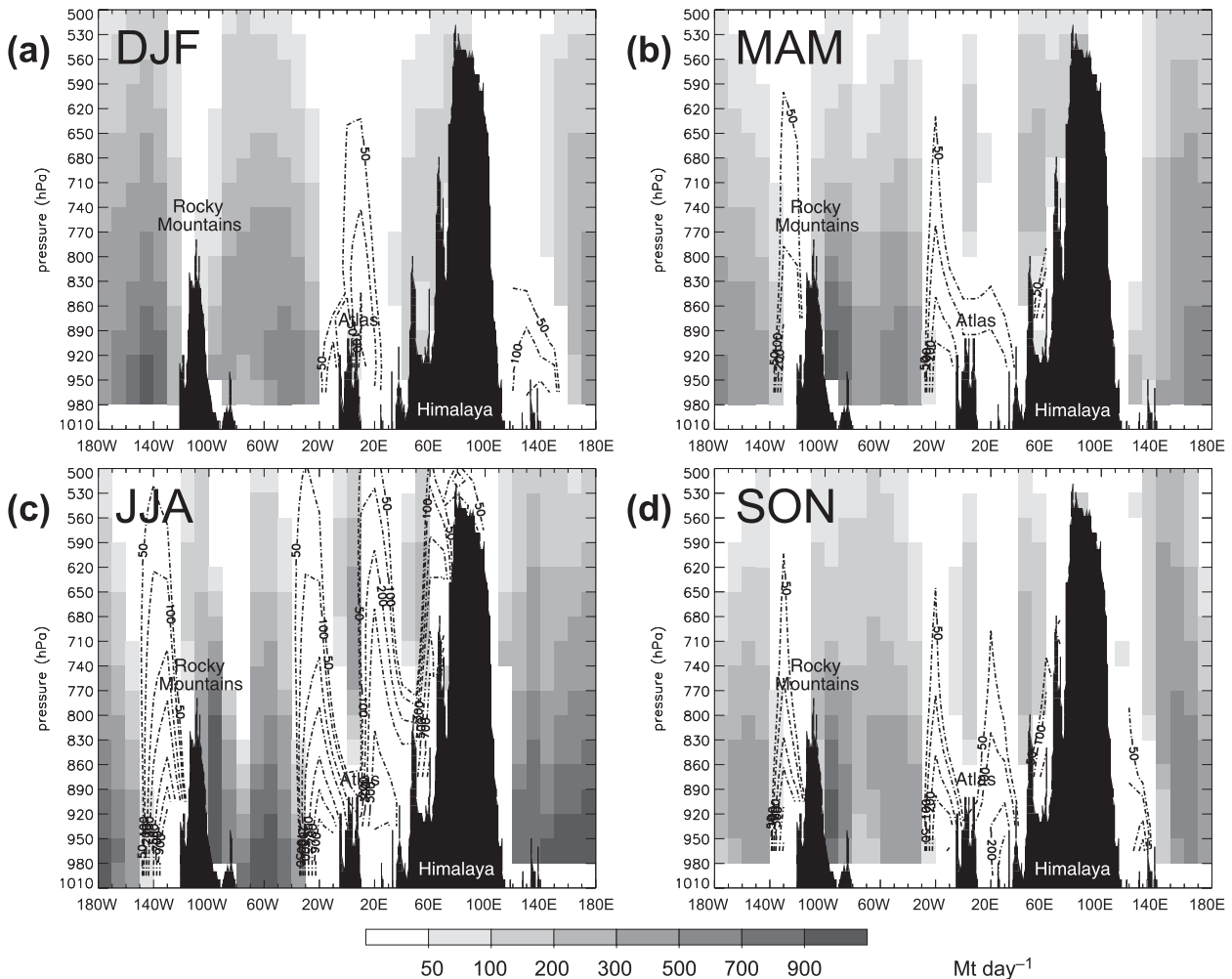E-mail: p.knippertz@leeds.ac.uk

FIG. 1. Zonal cross sections along 35°N showing climatological values of meridional water vapor transport across 30 hPa by 10° longitude boxes, calculated from ERA-40 for the period 1979–2001; units are Mt day^{-1}. Shading indicates poleward, dashed contours equatorward transport. Blackened areas show ECMWF model orography in 1° resolution with main mountain features labeled. Note that parts of the lowest boxes are occasionally below ground, resulting in overall low values.

indications of a splitting of the northward transport into a strong narrow branch over the Great Plains of North America and one broader branch over the western Atlantic, in particular in summer (Fig. 1c). The Pacific basin shows a more complicated seasonal behavior. In analogy with the Atlantic, there is a general tendency of equatorward transport at the eastern edge and poleward transport farther west. However, the maximum of the latter shifts eastward from winter through spring into summer and then shows a double maximum in autumn. At the western edge over East Asia, the transport direction changes from poleward in summer and spring (Figs. 1b,c) to equatorward in autumn and winter (Figs. 1a,d), reflecting the low-level wind reversal associated with the Asian monsoon.

A peculiarity of the moisture source regions associated with the marine subtropical highs is that the moist plan-

etary boundary layer (PBL) is usually rather shallow and capped by a deep and dry free troposphere caused by large-scale subsidence. This is reflected in a confinement of significant meridional moisture transports to below 800 hPa in the regions with southerly transport, except during summer when the subtropical highs shift poleward and moisture transports increase almost everywhere in magnitude and vertical extent with respect to the other seasons. The tendency of the poleward transports to occur in a deeper layer than the equatorward transports indicates that midlatitude weather systems lift moist air masses out of the subtropical PBL. This is clearly evident for the Atlas Mountains where the low-level trade winds over the eastern Atlantic and the harmattan winds over the African continent transport moisture equatorward while upper-level disturbances from the extratropics instigate upward

and poleward transports aloft (Figs. 1b–d; Knippertz et al. 2003; Knippertz 2003).

On synoptic time scales, transient circulation features can regionally instigate a direct transport of moist tropical air masses into midlatitudes. In such cases, the moist layers are often deeper than in purely subtropical air masses and can lead to heavy precipitation (e.g., Higgins et al. 2000; Cavazos and Rivas 2004; Bao et al. 2006; Stohl et al. 2008) and strong latent heat release in the extratropics, which in turn can contribute to explosive cyclogenesis (e.g., Reed et al. 1988; Zhu and Newell 1994). The regions of intense poleward moisture fluxes are often longitudinally quite narrow and have therefore been named atmospheric or tropospheric rivers (Newell et al. 1992; Newell and Zhu 1994; Zhu and Newell 1994, 1998; Ralph et al. 2004), a term later criticized by Wernli (1997) and Bao et al. (2006). Instead, Bao et al. (2006), and Knippertz and Martin (2007, KM07 hereafter) suggested the term "moisture conveyor belt" to stress the analogy with the well-established conveyor belt model of extratropical cyclones (Carlson 1980; Browning 1990). In contrast to the classical "warm conveyor belt" (WCB) concept, which includes a slow rise of PBL air from within the warm sector over the surface cold or warm front (e.g., Eckhardt et al. 2004), KM07 noticed in their case study that most moist trajectories with tropical origins followed a quasi-horizontal poleward track above the PBL and then rose abruptly in the precipitation zone.

A fairly frequent example of a link between tropical humidity and extratropical precipitation is colloquially known as the "pineapple express," which is characterized by a strong and persistent flow of atmospheric moisture and associated heavy rainfall from the waters adjacent to the Hawaiian Islands and extending to any location along the Pacific coast of North America (Higgins et al. 2000; Cavazos and Rivas 2004). Pineapple express (PE) situations usually occur during the winter half year (see maximum around 150°W in Fig. 1a) and can be associated with substantial flooding (Mass 2008). Other examples of tropical moisture feeding unusual extratropical rain events have been discussed for the easternmost North Pacific (Bao et al. 2006; KM07), for northwestern Africa (Fink and Knippertz 2003; Knippertz and Martin 2005), and even for northern Europe (Stohl et al. 2008). A more persistent and rather stationary feature of a tropical moisture–precipitation link develops over East Asia in summer and has been referred to as the mei-yu–baiu front that brings heavy rainfalls to parts of China, South Korea, and Japan (e.g., chapters 3 and 4 in Chang and Krishnamurti 1987; Ninomiya and Shibagaki 2007). It is clearly reflected in Fig. 1c in large transports between 110° and 130°E.

In this paper, the authors will refer to the whole class of such phenomena as "tropical moisture export" (TME) events. For the first time, an objective climatology of TME will be presented based on more than 1.25 billion trajectories calculated from 40-yr European Centre for Medium-Range Weather Forecasts (ECMWF) Re-Analysis (ERA-40) data. The study provides a comprehensive account of TME frequency, geographical, seasonal, and interannual variations as well as contributions to climatological moisture transports and precipitation. After describing the data and trajectory method used to identify TME events in section 2, some exemplary case studies are presented in section 3 to illustrate the influence of TME on both precipitation and cyclone intensification in the extratropics. Sections 4 and 5 contain detailed statistical analyses of spatial and temporal variations of TME trajectories and associated moisture transports, respectively, while section 6 focuses on the climatological contribution of TME to precipitation in the extratropics. Finally, main conclusions and ideas for future research on this topic are given in section 7.

2. Data and method

The results of this study are mainly based upon 6-hourly ERA-40 data (Uppala et al. 2005) for the 23-year period 1979–2001, which are available on 60 model levels and have been interpolated from the native $T_L 159$ to a regular grid with $1° \times 1°$ horizontal resolution. For studying cases after the ERA-40 period, ECMWF operational analyses interpolated to the same horizontal resolution have been used (native resolutions are T511L60/T799L91 before/after February 2006). To identify TMEs, trajectories are calculated with the software package Lagrangian Analysis Tool (LAGRANTO; Wernli 1997; Wernli and Davies 1997), which allows tracing different meteorological parameters along the trajectories by interpolating the respective fields to the position of the trajectory at a given time. The identification procedure of TMEs consists of three steps that account for their most important characteristics (see schematic depiction in Fig. 2:

- Step 1: Moisture source in the tropics—For every 0000 UTC analysis time, one-day forward trajectories are calculated from every 100 km $\times$ 100 km $\times$ 30 hPa box between 0° and 20°N, and between 1000 and 490 hPa. As every trajectory represents the same atmospheric mass of $\sim 3 \times 10^{12}$ kg, specific humidity can be readily converted into water mass. The upper boundary of the starting region for the trajectories was set to 490 hPa, as about 90% of all water vapor is
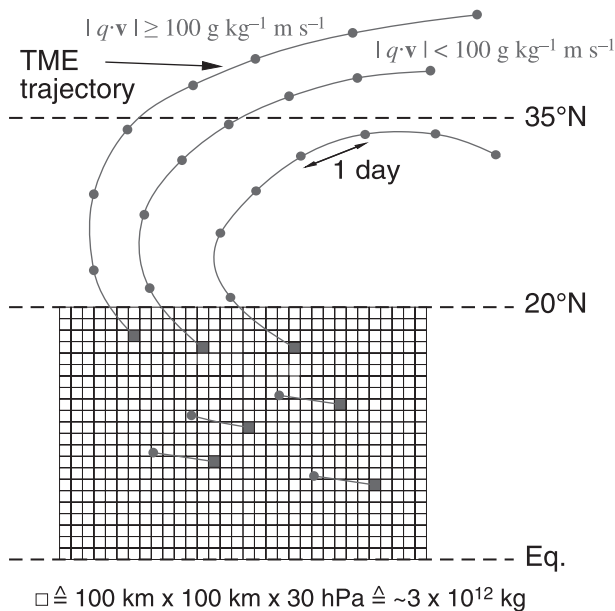
FIG. 2. Schematic illustration of the TME trajectory identification algorithm. Trajectories are started from each box at 0000 UTC every day. To avoid a double counting of air parcels on similar trajectories, only those that cross 20°N during the first 24 h are run forward in time for another 6 days. The seven examples starting from the gray boxes illustrate typical types of trajectory behavior. The only trajectory that is identified as a TME trajectory is the one that reaches a water vapor flux of at least 100 g kg^{-1} m s^{-1} to the north of 35°N. For more details, see section 2.

concentrated below this level. These trajectories can be expected to represent the synoptic-scale atmospheric flow well, but might be less reliable in regions of active tropical convection.

- Step 2: Poleward circulation—Out of the ~150 000 one-day trajectories started daily (more than 1.25 billion for the whole period) only those that cross 20°N are continued for another six days. If they reach 35°N within this period, they are retained. This relatively short time span was chosen to ensure that the considered air parcels are likely to maintain characteristics of tropical air on their way across the subtropics, although we cannot exclude that some parcels will undergo modifications due to fluxes of heat and moisture from the underlying surface or through mixing with ambient air. The minimum average meridional wind speed consistent with this criterion is 2.85 m s^{-1}.

- Step 3: Significant moisture transport into the extratropics—Finally, only those trajectories are retained that reach a water vapor flux of at least 100 g kg^{-1} m s^{-1} somewhere north of 35°N. Such a flux criterion selects for "fast" events, but tests with a mixing ratio criterion instead showed rather similar results. While the geographical distribution is generally quite robust, the number of trajectories varies non-

linearly with the chosen threshold (e.g., reduction by almost 80% for a doubling of the threshold). The value of 100 g kg^{-1} m s^{-1} was set in order to get robust, yet meaningful statistics.

In addition to ECMWF products, global monthly Climate Prediction Center (CPC) Merged Analysis of Precipitation (CMAP) data in 1° × 1° horizontal resolution for the 24-year period 1979–2002 (Xie and Arkin 1996, 1997) have been used to estimate the contribution of TME-related precipitation to climatological values (see section 6). For the example cases discussed in section 3, the Tropical Rainfall Measuring Mission (TRMM) and other data precipitation (3B42 V6; Huffman et al. 2007) in a spatial resolution of 0.25° has been considered on a daily basis. These combined microwave–infrared estimates (with gauge adjustment) were downloaded from http://disc2.nascom.nasa.gov/Giovanni/tovas/ operated by the National Aeronautics and Space Administration.

3. Exemplary case studies

To illustrate some typical characteristics of TME events, Fig. 3 shows all identified trajectories for 22, 24, 26, and 28 November 2001, when both the Pacific and Atlantic storm tracks were very active. To facilitate reference in the text, the four coherent TME regions are numbered as TME1–4. TME1 over the western North Pacific consists of a fairly small number of 24 (293) trajectories on 22 (24) November 2001 (Figs. 3a,b). They show the typical anticyclonic curvature when circulating from the tropical low-level easterlies into the midlatitude westerlies (KM07). The pertinent box-and-whisker plot in Fig. 3b demonstrates that the trajectories originate from a shallow layer of the tropical troposphere (median is ~940 hPa). The tracks are initially quasi-horizontal and then rise abruptly near 35°N, 165°E to about 500 hPa, where they remain until 28 November. According to the TRMM daily rainfall product (not shown), precipitation associated with this feature was widespread but of moderate intensity, consistent with the small number of TME trajectories.

TME2 is rooted over the eastern half of the North Pacific and persists throughout all four analysis times shown in Fig. 3. The number of trajectories forming TME2 increases from 790 (752) on 22 (24) November to an unusually high value of 1971 on 26 November and then decreases to 715 on 28 November. Trajectory origins are from a deep layer of the tropical troposphere (median ~790 hPa); tracks are initially quasi-horizontal or even subsiding (insets in Figs. 3a–c). The trajectories subsequently pass a region of strong ascent, mainly on
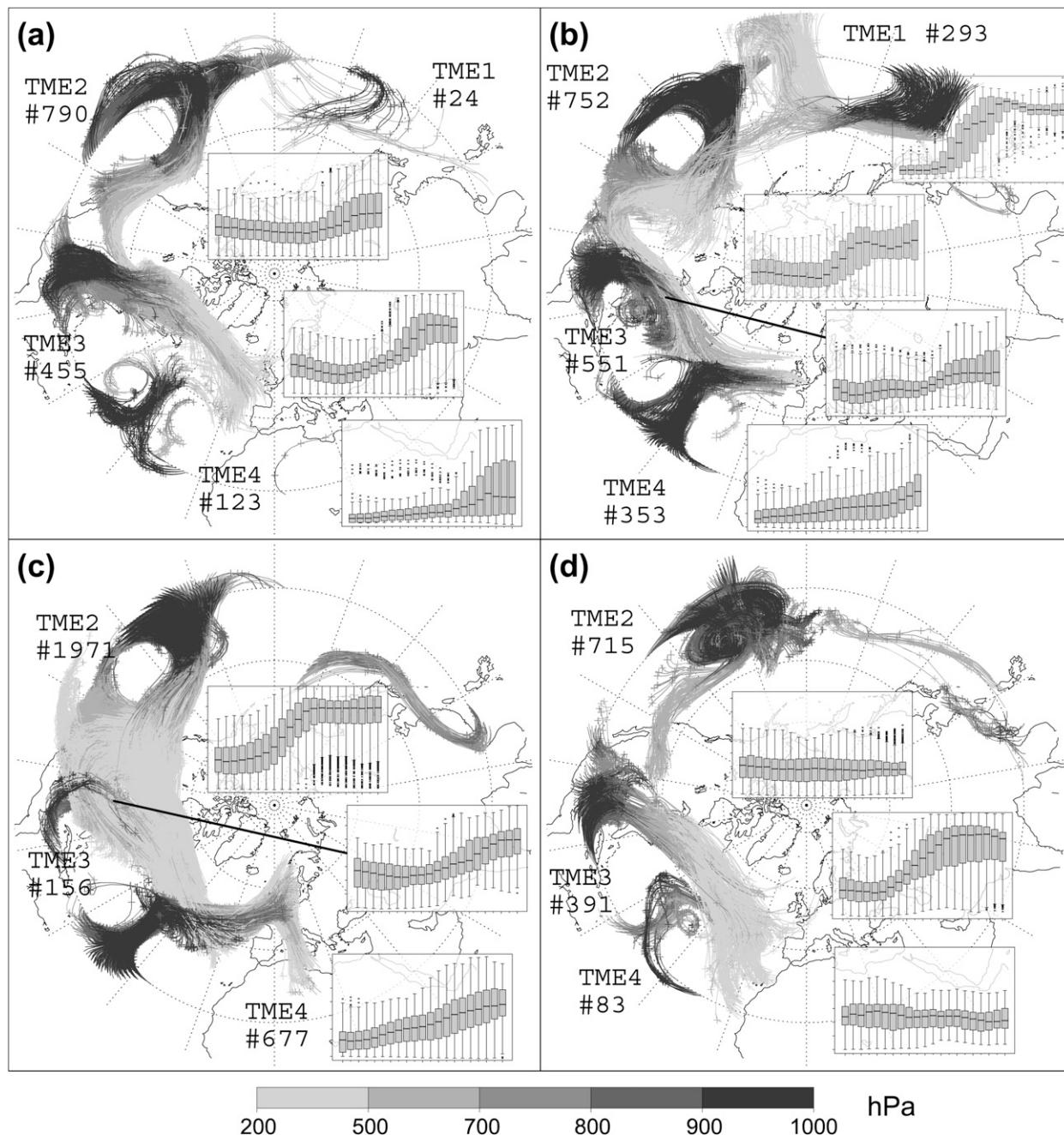
FIG. 3. TME trajectories started at 0000 UTC (a) 22, (b) 24, (c) 26, and (d) 28 Nov 2001. Gray shading indicates the height of the trajectories in hPa. For each coherent feature with more than 80 trajectories (numbered TME1–4), the insets show a box-and-whisker depiction (thick line median, box interquartile range, crosses outliers) of the trajectory heights (from 1000 to 300 hPa) as a function of trajectory calculation time every 6 h. The whiskers extend to the most extreme data point, which is no more than 1.5 times the interquartile range from the box. The number of identified TME trajectories is also given for each coherent feature. For the sake of clarity, only the first five days of the trajectories are plotted.

26 November in Fig. 3b and on 27–28 November in Fig. 3c. Associated with this ascent is a precipitation band reaching from the ITCZ near 160°W across the Hawaiian Islands all the way to the Pacific Northwest,

typical of a pineapple express situation. According to TRMM data, 48-h sums on 27–28 November 2001 exceeded 200 mm and locally even 300 mm in the area of Hawaii (not shown). This is consistent with observations

of 231 mm at Hilo airport and flash flooding on the big island of Hawaii. Flash flooding also occurred in northern California, and several rivers and streams in Oregon showed rapid rises in response to widespread precipitation of more than 70 mm [National Weather Service (NWS) flood summary is available online at http://www.weather.gov/oh/hic/archive/2001/011129.htm]. As for TME1 there is a bifurcation into a westerly branch and one returning to low latitudes at later stages (Figs. 3b,c). Other examples of particularly hazardous pineapple expresses (see Mass 2008) also show TME contributions. The period of 4–8 February 1996 with a rather high number of 1249 TME trajectories was associated with more than twice the monthly precipitation, some rainfall records, and substantial flooding in some regions along the west coast of North America (not shown). The record flood peak event of 5–7 November 2006 in the Pacific Northwest had contributions from 1196 TME trajectories.

TME3 is already fully developed on 22 November 2001 and indicates substantial moisture transports from the Caribbean into the eastern United States with 455 TME trajectories, which sharply rise on 25 November (Fig. 3a). On 24 November, TME3 comprises 551 trajectories that ascend less (Fig. 3b). TME3 weakens to 156 trajectories on 26 November and then reintensifies on 28 November to 391 trajectories, which mainly rise on 29–30 November (Figs. 3c,d). This episode was associated with record rainfall in the midsouth with storm totals for 26–29 November of 200–300 mm common throughout the area, according to the U.S. National Weather Service. This resulted in extensive flash flooding, inundation of homes and buildings, washed-out roads, and one fatality. The amount of 174 mm that fell in Memphis, Tennessee, between 0600 UTC 28 November and 0600 UTC 29 November was the highest 24-h total recorded since October 1935. The 180 mm in Jackson, Mississippi, on 28–29 November 2001 is the second wettest 48-h period on record. Interestingly, the 48-h record of 198 mm on 24–25 December 1987 was also related to considerable TME (not shown). TME4 over the central North Atlantic is also present through the entire period with 123, 353, 677, and 83 identified trajectories, respectively (Fig. 3). Compared to TMEs1–3, the ascent within TME4 is fairly moderate and the median stays below 600 hPa. Consistently, only light precipitation is associated with this feature. In addition to TMEs1–4, the algorithm also identifies several TME trajectories that originate near China and one unusual trajectory over the Sahara in Fig. 3a. The foregoing discussion demonstrates that TMEs are usually both spatially and temporally coherent airstreams that can (but do not necessarily) contribute to heavy precipitation events in the extratropics.

A very recent example of a possible influence of TME on rapid extratropical cyclogenesis is the intense storm Klaus that hit northern Spain and southwestern France on 24 January 2009 with gusts of more than 150 km h^{-1} at low-elevation stations, torrential rains, and flooding, leading to some casualties and insured losses of several hundred million euros. The storm developed over the Atlantic Ocean on 22 and 23 January, moved very rapidly in the strong westerly flow, and reached the east coast of France just before 0600 UTC on 24 January (see track in Fig. 4). Between 0000 and 1200 UTC on 23 January the core pressure fell from 1001 to 973 hPa and finally even to 963 hPa 12 h later. Accounting for the relatively low latitude of the track, this corresponds to a geostrophically equivalent rate of 1.9 Bergeron (see Sanders and Gyakum 1980). The operational ECMWF model underestimated this explosive deepening even at short lead times (T. Hewson, ECMWF, 2009, personal communication). The TME trajectory analysis for 0000 UTC 19 January to 0000 UTC 24 January shows that the development of Klaus was embedded in a massive TME event with an unusually high number of 1685 TME trajectories, which originate over the entire central and western tropical Atlantic and then converge into the genesis region of Klaus (Fig. 4). It appears quite conceivable that latent heat release in this moist and warm air mass served as an additional diabatic energy source to the baroclinic development, although only a fraction of the many trajectories ascended all the way to the tropopause (inset in Fig. 4). A more detailed dynamical analysis of this event and an estimation of the number of extratropical cyclones that are directly affected by TME are beyond the scope of this paper and left for future study.

4. Trajectory counts and characteristics

This section contains a statistical analysis of the three-dimensional and seasonal variations of TMEs together with their associated moisture and wind speed anomalies. All results are presented in the form of zonal cross sections with all statistics calculated for boxes that extend 30 hPa in the vertical and 10° in the zonal direction.

a. Longitudinal, vertical, and seasonal distribution

Figure 5 shows zonal cross sections along 35°N with counts of TME trajectories for the four seasons December–February (DJF), March–May (MAM), June–August (JJA), and September–November (SON). TME is mostly restricted to longitudinally confined regions with low orography in the subtropics. The most prominent are the following:
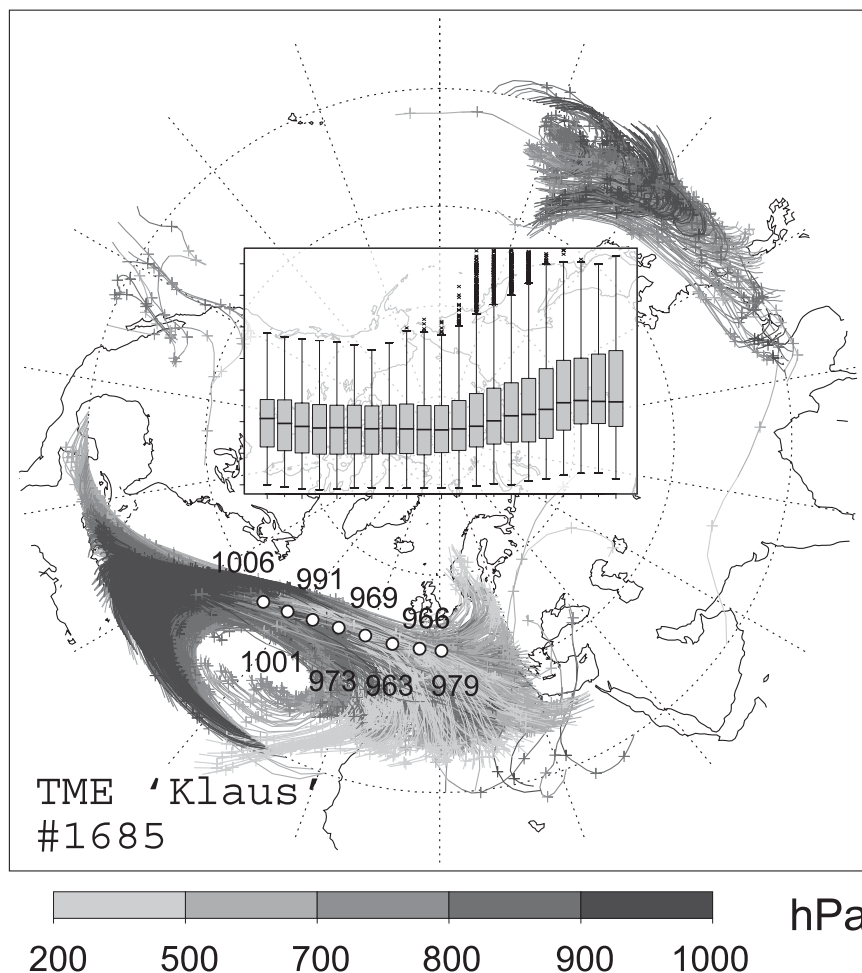
FIG. 4. As in Fig. 3, but for TME trajectories started at 0000 UTC 19 Jan 2009. The 6-hourly position of the intense cyclone Klaus with the associated core pressure (hPa) between 1800 UTC 22 Jan and 1200 UTC 24 Jan are given as filled circles and numbers, respectively. Note that operational ECMWF analyses were used for this figure since the date of the event is after the end of the ERA-40 period.

(i) The previously discussed pineapple express (marked "PE" in Figs. 5a,d), which connects the tropics near Hawaii with the North American west coast (see TME2 in Fig. 3 for an example). It has a clear activity maximum in DJF and is practically absent in JJA. The PE is ill defined in MAM and appears as a weak local maximum of more than 250 trajectory counts at 160°–150°W, 800–680 hPa in SON. The low activity in summer is consistent with the then strong and persistent subtropical anticyclone over the eastern North Pacific that effectively impedes poleward moisture transports.

(ii) A second prominent hotspot is the west Pacific (WP in Fig. 5), which is active from MAM to SON with a clear maximum in JJA when the main activity shifts westward from ~150°E to ~130°E. In all three seasons there are considerable trajectory counts throughout the lowest 500 hPa of the atmosphere with maxima around 700 hPa in SON and DJF, and below 800 hPa in JJA. The summer maximum is presumably closely related to the mei-yu–baiu front over East Asia (see section 1). An example is TME1 in Fig. 3.

(iii) A locally very confined maximum occurs between the Rocky and the Appalachian Mountains and is therefore termed "Great Plains" (GP in Figs. 5b–d). It is the sole continental TME activity maximum and is mainly restricted to the 100°–90°W strip. Its seasonality resembles the one of WP with a maximum of more than 1500 trajectories in summer and rather weak activity in winter. The inflow of moist air masses from the Gulf of Mexico into the central parts of the United States is related to the North American monsoon system (e.g., Adams and
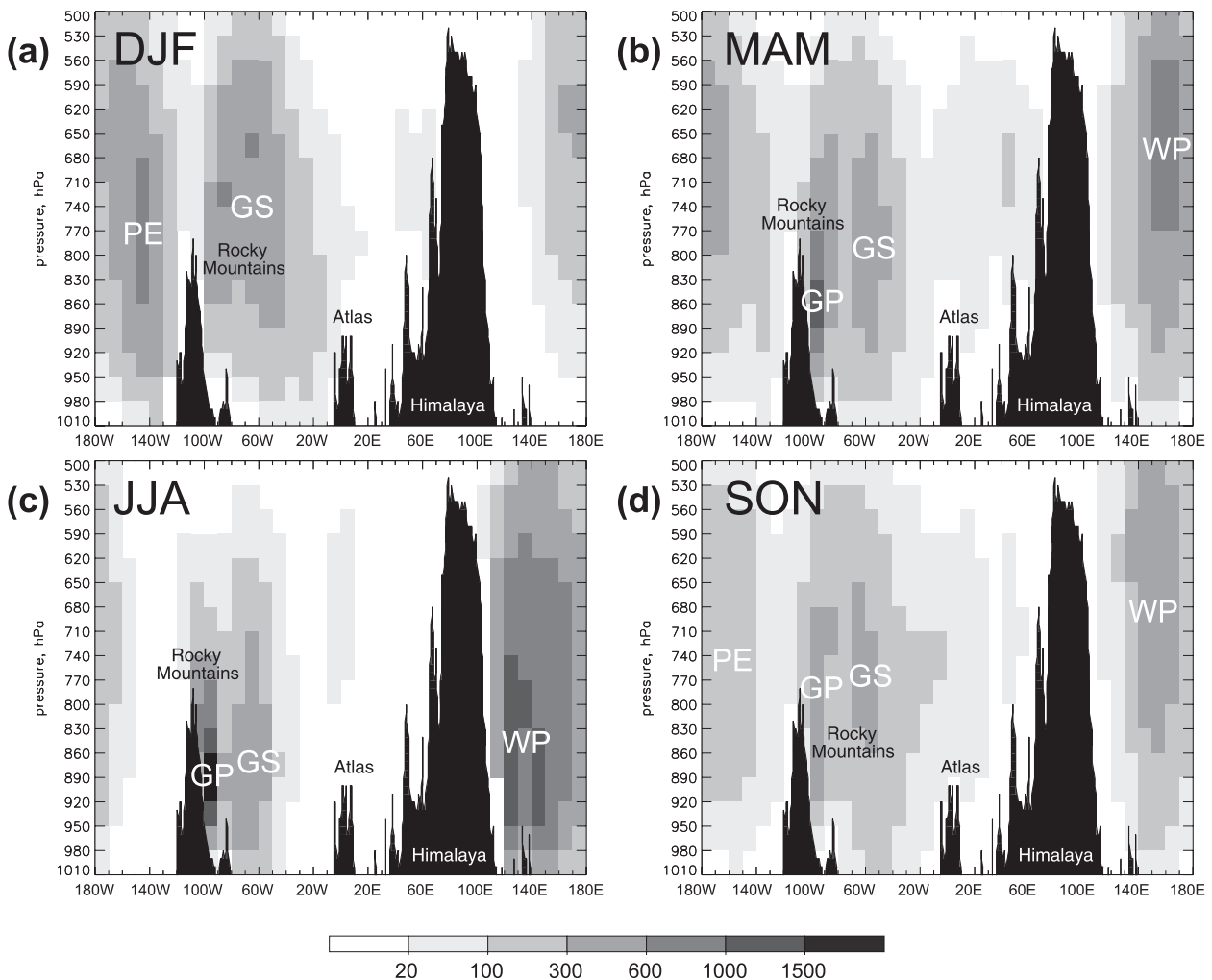
FIG. 5. Zonal cross sections along 35°N showing counts of TME trajectories in 30 hPa by 10° longitude boxes over the period 1979–2001 for (a) DJF, (b) MAM, (c) JJA, and (d) SON. Blackened areas show ECMWF model orography in 1° resolution with main mountain features labeled. The most significant TME regions are labeled PE, GP, GS, and WP. Note that parts of the lowest boxes are occasionally below ground, resulting in overall low counts.

Comrie 1997) and is intimately linked to convective activity in this region as shown by the example TME3 in Fig. 3.

(iv) The fourth prominent TME activity maximum is located over the western inflow region of the North Atlantic storm track along the east coast of North America and is therefore termed "Gulf Stream" (GS in Fig. 5). It is active year-round and has a much smaller annual cycle than regions i–iii, which is mainly reflected in a weakened activity in summer and a higher elevation in DJF.

b. Mean characteristics of TME trajectories

To test whether TMEs constitute predominantly a moisture or a circulation anomaly, Fig. 6 shows mean specific humidity and meridional wind averaged over all identified trajectories in a given longitude–pressure box (shading) together with the climatological averages calculated for the entire ERA-40 period 1957–2002 (lines). For DJF, TMEs in both the PE and GS regions show values of more than 6 g kg^{-1} throughout the bottom 150 hPa of the atmosphere (Fig. 6a). Maximum values around 9 g kg^{-1} are found over the Atlantic. The climatological moisture field has an overall similar structure, but with smaller absolute values by about 1–3 g kg^{-1}. The most striking difference is the extension of the moist layer to well above ~800 hPa during TME. The corresponding meridional TME wind fields reach values up to 5.5 m s^{-1}, significantly more than the climatological values that hardly exceed 2 m s^{-1} (Fig. 6b). There is a general decrease of the meridional wind
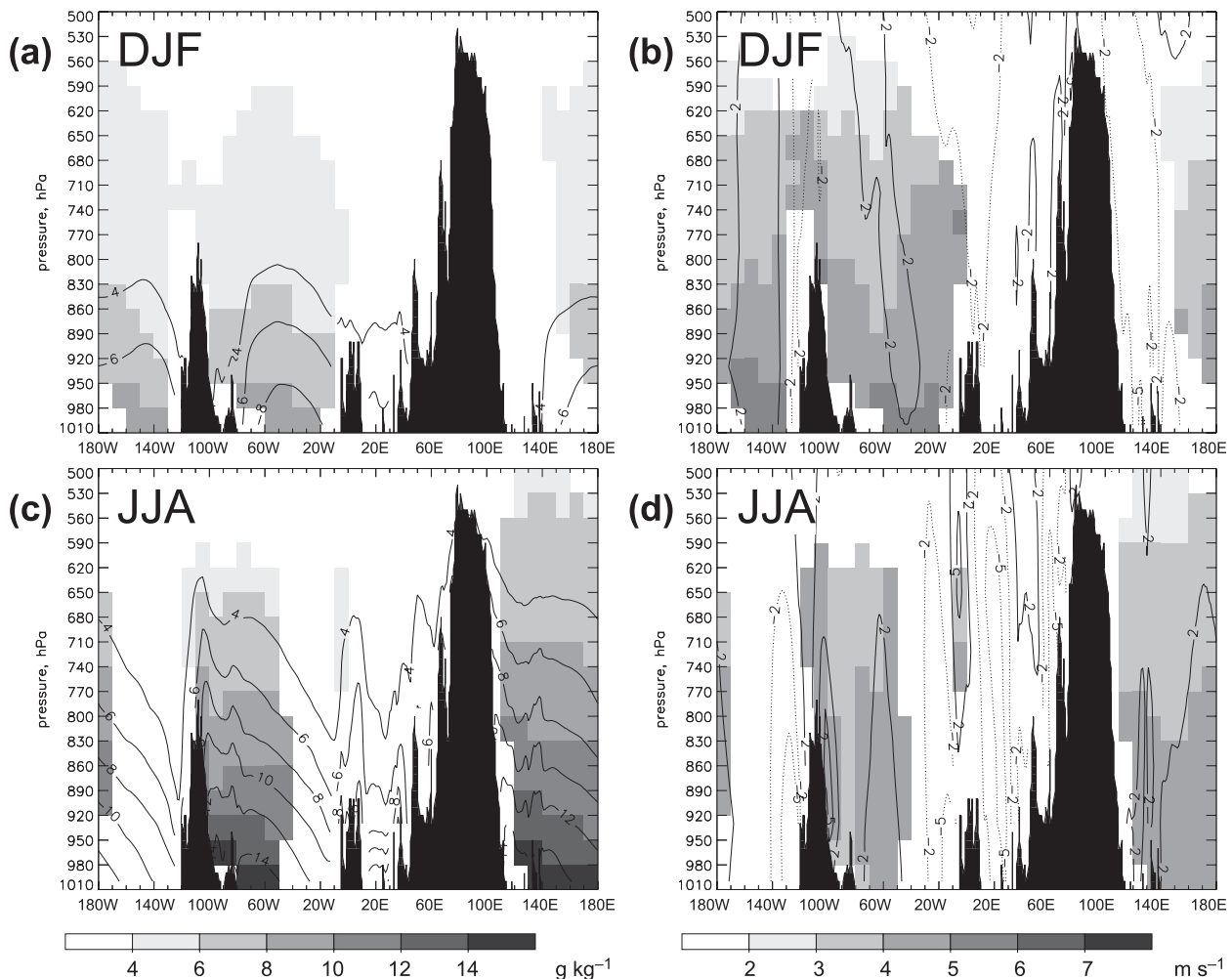
FIG. 6. (a) Mean specific humidity (g kg^{-1}) and (b) meridional wind (m s^{-1}) for TME trajectories crossing 35°N for DJF 1979–2001 (shading). Values are plotted for 30 hPa by 10° longitude boxes if they contain at least 30 trajectories. Lines indicate the respective climatological means calculated for the entire ERA-40 period 1957–2002. (c),(d) Same as (a) and (b), but for JJA.

component with height within the TMEs. TMEs are more frequently, but not exclusively, found in regions with climatological southerlies.

During summer a slightly different picture emerges. The absolute values of both climatological and TME specific humidity are much higher and reach 14 g kg^{-1}, but the differences between the two become very small below 800 hPa (Fig. 6c). This is a reflection of the overall weaker air mass contrasts during this season that make it more difficult to create a substantial anomaly in an already warm and moist environment. At higher levels TME anomalies locally exceed 3 g kg^{-1}. The meridional wind plot shows deep layers of southerlies around 4 m s^{-1} associated with TMEs in both the GP–GS and WP regions (Fig. 6d) and a smaller decrease with height than in winter. Compared to the climatological values around 2 m s^{-1}, TME winds are on the order of 2–3

times faster. An interesting exception is the low-level jet along the eastern side of the Rocky Mountains, where mean winds reach more than 4 m s^{-1}. In conclusion, Fig. 6 demonstrates that during all seasons TMEs are a combination of anomalous southerlies with anomalously high moisture contents with the importance of the latter decreasing in summer.

c. Latitudinal variations

Finally, latitudinal variations, and thereby in some sense also the time evolution, of TMEs are addressed by examining trajectory counts as in Fig. 3 in different zonal cross sections between 25° and 50°N (Fig. 7). Only results for the DJF season are shown, as they sufficiently illustrate the most important aspects. In a statistical sense, both PE and GS trajectories track almost straight northward between 25° and 30°N and are mostly confined
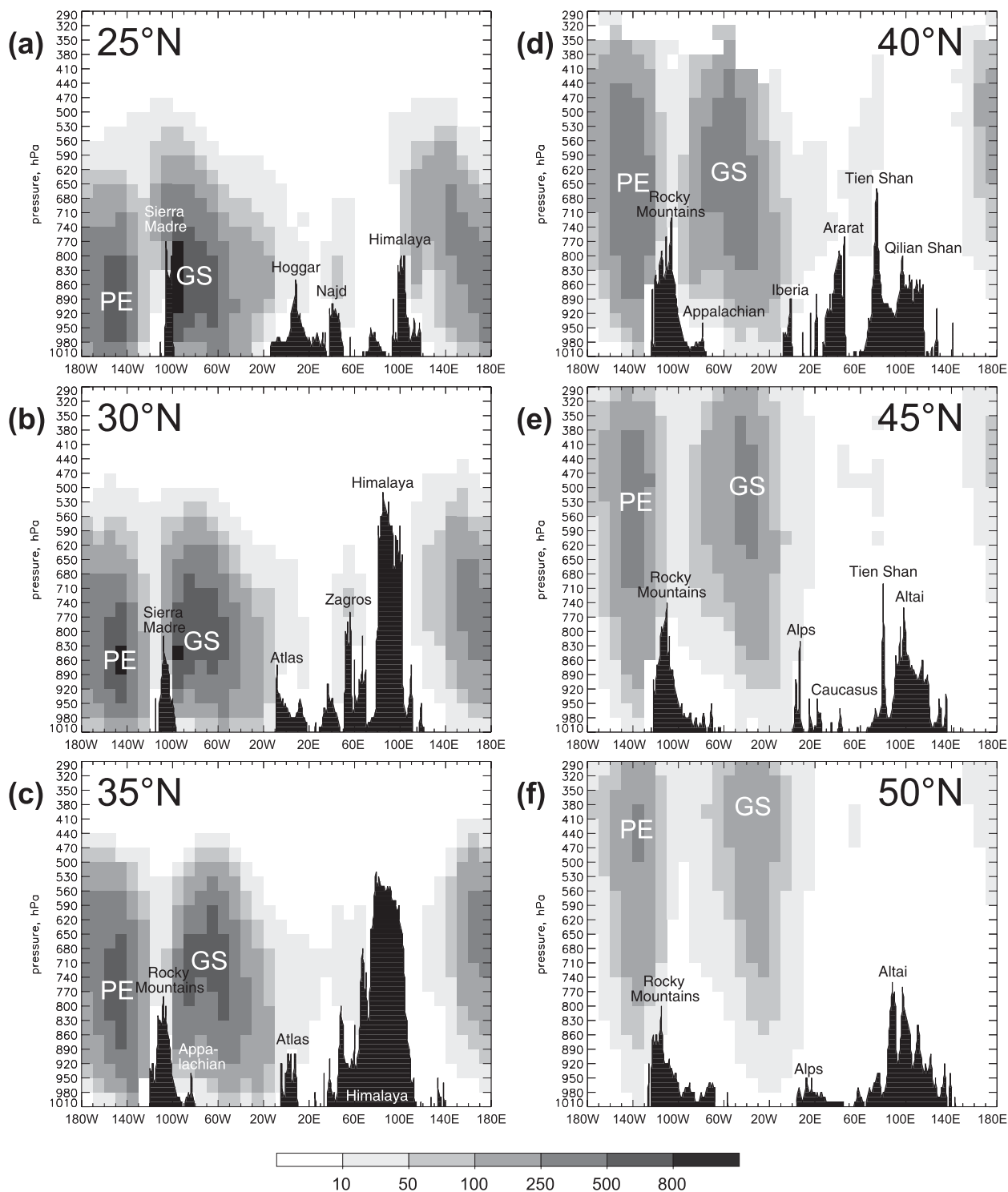
FIG. 7. Counts of TME trajectories crossing (a) 25°N, (b) 30°N, (c) 35°N, (d) 40°N, (e) 45°N, and (f) 50°N in 30-hPa by 10° longitude boxes for DJF 1979–2001. Labels are as in Fig. 5. Note the different vertical axis compared to Fig. 5.

to the layers below 500 hPa (Figs. 7a,b). Around 35°N trajectories begin to rise while still on an almost meridional track (Fig. 7c, note the different contour interval with respect to Fig. 5a). Between 35° and 45°N the PE trajectories rise over the western slopes of the U.S. Rocky Mountains, while GS trajectories show even stronger ascents into the midtroposphere, most likely related to WCBs of midlatitude baroclinic waves over the central North Atlantic (Figs. 7c–e). In both TME regions the tracks shift eastward by about 10°–20° longitude in this latitude band. At 50°N the overall numbers are largely reduced as many trajectories have recirculated toward low latitudes (as, e.g., TME1 in Fig. 3). Nevertheless, both ascent and eastward shift continue in this area. Trajectories in other seasons and regions also tend to slowly rise anticyclonically, although the ascending regions are shifted northward by about 5° in summer. In addition, Fig. 7 illustrates why the large area from 10°W to 120°E (i.e., more than a third of the earth's circumference) is practically void of TMEs: Poleward moisture transports in this region are hindered by orographic features in Africa, Asia, and Europe as indicated by the black ECMWF model orography.

5. Total moisture exports

While the foregoing discussion revealed the temporal and spatial characteristics of TMEs including the associated moisture and wind anomalies, it is not straightforward to translate this information into transported total water mass. To achieve this, the trajectory counts for each 30-hPa by 10° longitude box were combined with their respective specific humidity and meridional wind velocity to quantify total moisture export across a given latitude circle for a given time. The obtained values were vertically integrated from 1010 to 80 hPa by summing up the data from the respective thirty-one 30-hPa boxes and then converted to Mt day^{-1}. It should be noted that this analysis does not include transports of water in liquid or solid form but concentrates on the dominating horizontal transport of water vapor. In the following three subsections this parameter will be discussed with respect to seasonal, interannual, and latitudinal variations.

a. Seasonal variations

Figure 8 shows vertically integrated, TME-related water vapor transports across 35°N for the four seasons DJF, MAM, JJA, and SON. Table 1 gives the respective values longitudinally integrated over each of the four TME regions discussed in section 4a and marked with gray shading in Fig. 8. In addition, percentages of the climatological water vapor transports shown in Fig. 1 are
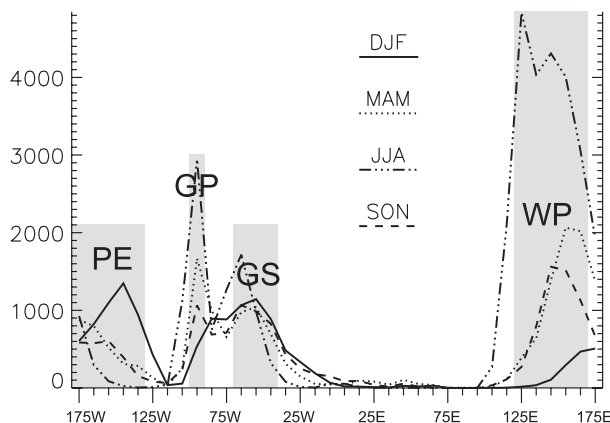

FIG. 8. Mean TME across 35°N in Mt day^{-1} per 10° longitude strip. Shown are the four seasons DJF (solid), MAM (dotted), JJA (dash–dotted), and SON (dashed) according to the legend. The water vapor exports are integrated between 1010 and 80 hPa. The four regions as defined in Table 1 are marked with gray shading.

given in Table 1. These data accentuate some of the aspects already discussed in section 4a. The activity maximum of the PE in winter (solid line), for example, becomes much clearer in this integral depiction than in Fig. 5. The maximum value for a single 10° longitude strip within the PE region is almost 1350 Mt day^{-1} in DJF, while in the other seasons values stay well below 1000 Mt day^{-1}. The total transports are about 2 times larger in DJF than in SON and MAM, and almost 4 times larger than in JJA (second line of Table 1). This picture changes completely, when relative contributions of TMEs to the total water vapor transported poleward across 35°N are considered. These values increase from winter (15.6%) over the transition seasons (22%–23%) to summer with 56.1%, when cancellation of transports in opposite directions causes a small climatological value (Fig. 1c).

GP water vapor exports are spatially confined to the immediate vicinity of the Rocky Mountains, that is, to the 100°–90°W longitudinal strip (Fig. 8). Maximum values of 2946 Mt day^{-1} occur during JJA, almost 2 times the MAM and 3 times the SON exports (Table 1). During DJF, transports are small, and the GP region appears more like a western extension of the GS region that is very active during this time of year (Fig. 8). Contributions to the climatological transports across 35°N range from 46.2% in summer over 27.1% in spring to 18.9% in autumn and 17% in winter (Table 1). This demonstrates the substantial importance of TME for the summer climate in the GP area. As pointed out in section 4, the GS region has by far the flattest annual cycle as revealed by total water vapor transports of between 3098 Mt day^{-1} in winter and 2713 Mt day^{-1} in spring

TABLE 1. TME across 35°N in Mt day^{-1} in the four main TME regions during the four seasons and in parentheses, percentage of the respective ERA-40 climatological values for the period 1979–2001 (see Fig. 1). Region abbreviations are as in Fig. 5 and spatial definitions are given in parentheses in the first column.

Region	DJF	MAM	JJA	SON
PE (180°–130°W)	4815 (15.6)	2791 (23.4)	1337 (56.1)	2316 (22.1)
GP (100°–90°W)	539 (17.0)	1667 (27.1)	2946 (46.2)	1064 (18.9)
GS (40°–70°W)	3098 (20.0)	2713 (19.4)	3019 (16.2)	2880 (24.9)
WP (120°–170°E)	924 (12.2)	6502 (28.9)	20 236 (54.1)	5269 (23.3)

(Table 1) with maximum 10° longitude values hardly exceeding 1200 Mt day^{-1} (Fig. 8). Because of the tendency of moister trajectories in summer (cf. Figs. 6a,c), the annual cycle is even flatter than in the TME trajectory counts (cf. Figs. 5a,c). Relative contributions are on the order of 16%–25% year-round (Table 1). It could be speculated that the comparably high values in autumn are related to the frequent recurvature of tropical cyclones into midlatitudes (Jones et al. 2003).

The WP is the region that dominates TME into the Northern Hemispheric extratropics during all seasons but DJF (Fig. 8). In JJA, transport in the entire region reaches 20 236 Mt day^{-1} with a 10° longitude maximum of 4835 Mt day^{-1} over the East China Sea (120°–130°E). This is 3–4 times the transition season values and more than 20 times the DJF transport (Table 1). The summer TME in the WP alone, which constitutes only 14% of the earth's circumference, is responsible for 61% (33%) of the global TME across 35°N in summer (over the entire year). The average daily TME of 20 236 Mt corresponds to ~1.4% of all water vapor contained between 10° and 20°N. Thus it would take only 10 weeks to empty the entire reservoir through the 50°-longitude-wide WP channel into the extratropics. With respect to the climatology, the WP contributions range from 54.1% in summer and over 23%–29% in the transition seasons to only 12.2% in winter. The WP and GP regions both show distinct TME maxima during Northern Hemispheric summer, when the sea surface temperatures (SSTs) are high and monsoon circulations are well established. In contrast, TME transports in the PE region are largest during a time of relatively low SSTs but when the active extratropical storm track frequently generates the circulation anomalies necessary for TME.

b. Interannual variations

Time series of the vertically and longitudinally integrated annual TME across 35°N show substantial year-to-year variations throughout the period 1979–2001 (Fig. 9). Note that for the regions with winter maxima (PE and GS) years run from July to June of the following year, while for the other two regions calendar years were used. Largest variability is found in the PE region, where

the most active year (1983/84) has an almost 3 times larger TME than the least active (1987/88), pointing to marked differences in the large-scale circulation over the eastern and central North Pacific (see discussion at the end of this subsection). Despite the smaller longitudinal range, the GP time series shows somewhat less fluctuation than PE with most years varying between 1000 and 1600 Mt day^{-1}. In the GS region the year-to-year range is 2150–4200 Mt day^{-1}. The WP region has, of course, the largest absolute values ranging from 6100–10 400 Mt day^{-1}, indicating moderate relative interannual fluctuations.

The calculation of simple linear correlation coefficients between the time series shown in Fig. 9 reveals limited coherence between the regions. This does not change markedly, if July–June, calendar years, or seasonal values are used for all time series. Only for the two regions over the eastern and western North Pacific (i.e., WP and PE), a significant correlation of −0.54 was found. There is also a weak negative correlation between GP and GS from MAM to SON. Annual and seasonal correlations with large-scale climate indices
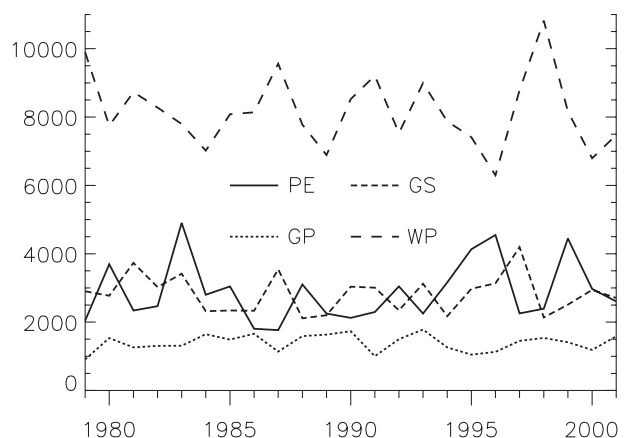

FIG. 9. Time series of 1010–80-hPa vertically integrated TME across 35°N in Mt day^{-1} for the four TME regions PE, GP, GS, and WP. Definitions of the regions are as given in Table 1 and gray shaded in Fig. 8 (note the different longitudinal width). Because of the different seasonality in the four TME regions, years for PE and GS stand for July to June of the following year, while years for GP and WP stand for calendar years.

like the North Atlantic Oscillation index (normalized surface pressure difference between the Azores/Gibraltar and Iceland; see Jones et al. 1997) and the Niño-3.4 index (SST anomaly in the region 5°N–5°S, 170°–120°W) give also rather low values. The exceptions worth mentioning are significant correlations between Niño-3.4 and TMEs in the GS (+0.47 on a July–June and +0.45 on a winter basis) and PE regions (−0.50 July–June and −0.35 winter).

It is remarkable to note that the TME anomalies over the PE are in opposite phase with the SST anomalies associated with the Niño-3.4 variations, that is, more (less) TME occurs when tropical SSTs are colder (warmer). This indicates that SST-induced circulation anomalies essentially modify the intensity of TME, while increases in column water vapor over the warmer ocean surface play a minor role. The negative correlation in the PE region is therefore most likely related to the well-known eastward extension of the North Pacific waveguide that inhibits the penetration of Rossby wave energy into low latitudes (Matthews and Kiladis 1999) and is associated with reduced anticyclonic wave breaking [or life cycle (of a baroclinic wave; LC1) events; Shapiro et al. 2001] and fewer tropical plumes (McGuirk et al. 1987; Iskenderian 1995). The positive correlation in the GS region is consistent with the "Mexican connection" proposed by Rasmusson and Mo (1993) that links Pacific SST anomalies with circulation anomalies over the western subtropical Atlantic and the Caribbean, where the number of tropical plumes is increased in El Niño years (Iskenderian 1995). In conclusion, these results suggest that TME is to some degree constrained by El Niño–induced circulation anomalies, while linkages between the individual TME regions are rather weak.

c. Latitudinal variations

The dependence of vertically integrated TME on latitude is shown in Fig. 10, using sections every 5° between 25° and 50°N as in Fig. 7. We only show results for summer and winter, since little additional insight is gained from the transition seasons. In winter, TME total water vapor transports fluctuate around 1200 Mt day^{-1} between 25° and 35°N in both the PE and GS regions. The slight increase in PE indicates a net moisture uptake (Fig. 10a). Between 35° and 50°N, TME trajectories lose about 50%–60% of their associated moisture flux, consistent with the ascending motions evident from Fig. 7. This indicates a substantial contribution to precipitation in this latitude strip as further discussed in section 6. Note the eastward shift of 20°–30° longitude of both activity maxima on their way from the tropics to 50°N as mentioned earlier. The summertime GP region exhibits a
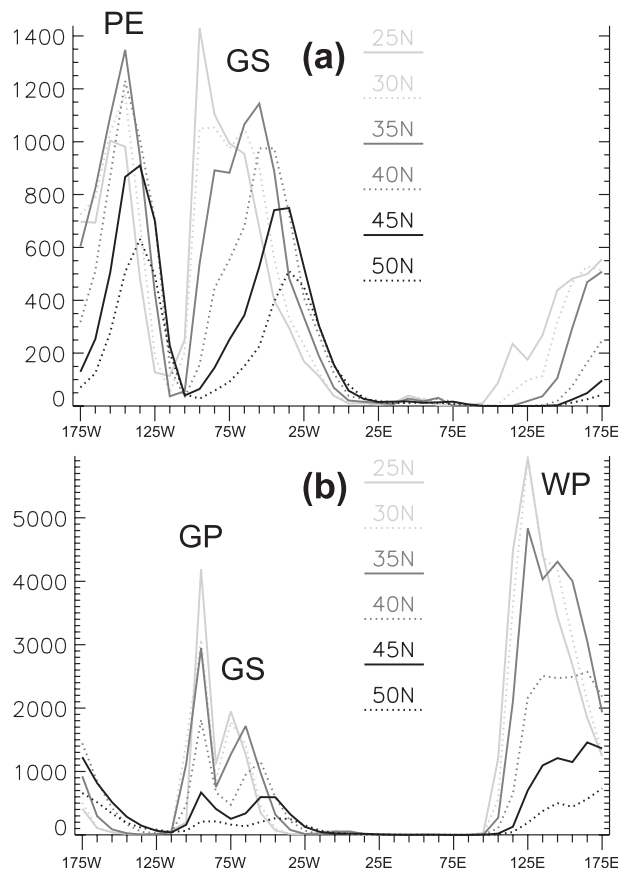

FIG. 10. Mean TME across different latitude circles (see legend) for (a) DJF and (b) JJA in Mt day^{-1} per 10° longitude strip. The water vapor exports are integrated between 1010 and 80 hPa. The most significant TME regions are labeled as in Fig. 5. Note the different ordinates in (a) and (b).

monotonous decrease in water vapor transport between 25° and 50°N with a dramatic drop in moisture flux on the order of 70% between 35° and 45°N (Fig. 10b). The eastward shift is weaker compared to PE and GS in winter. The water vapor flux over the WP decreases more slowly between 25° and 35°N and then also drops by about 70% between 35° and 45°N. These results indicate an even more substantial contribution to precipitation as will be shown in the following section. The eastward shift with latitude is comparable to PE and GS in winter.

6. TMEs and precipitation

The latitudinal dependence of TME water vapor transports presented in section 5c has already given some indications on the importance of this phenomenon for extratropical precipitation. Here this aspect is further quantified by summing water vapor losses along TME trajectories in 2° × 2° latitude–longitude boxes to obtain an estimate of TME-related precipitation in millimeters
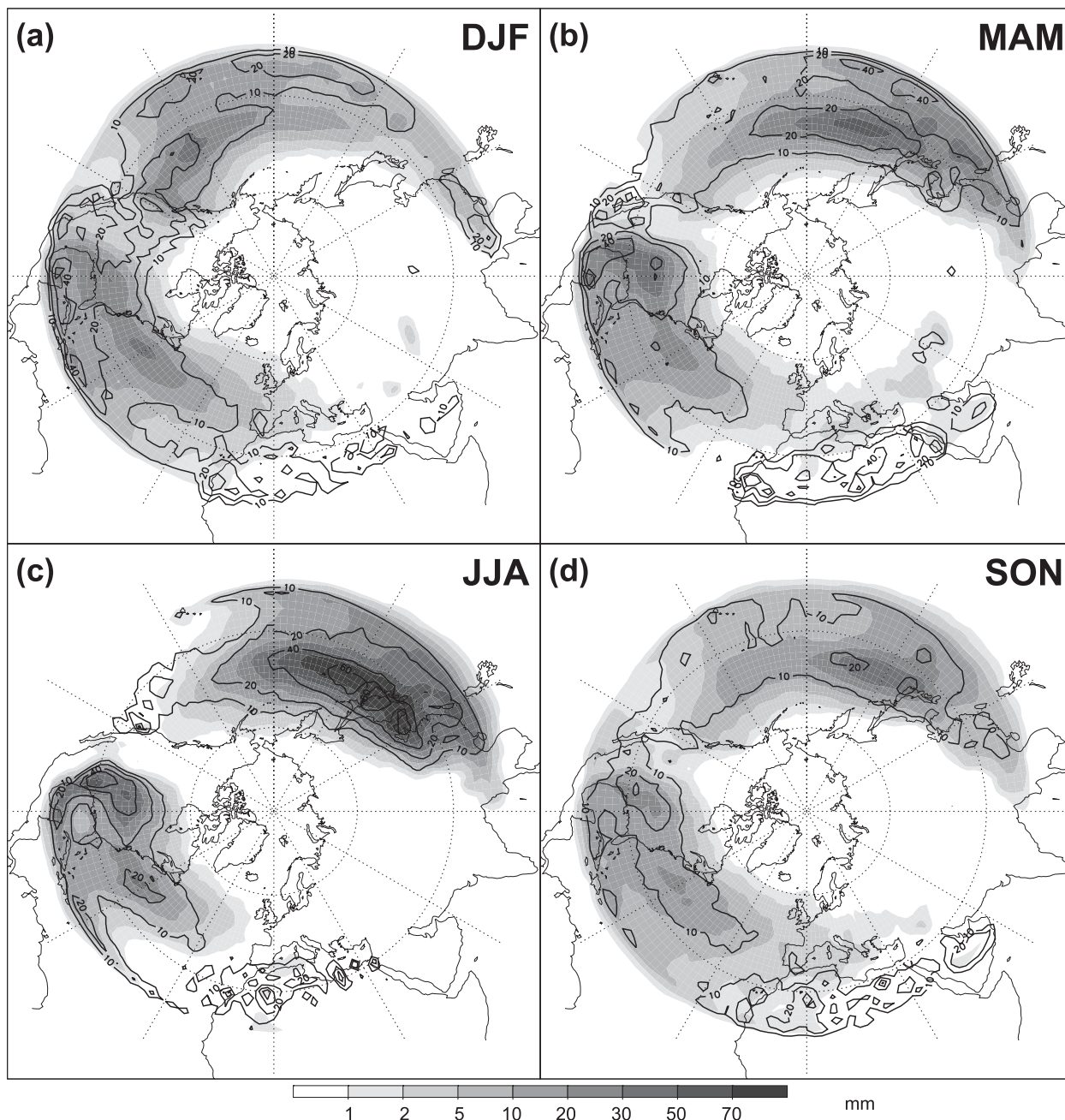
FIG. 11. TME-related precipitation calculated from moisture losses along TME trajectories in millimeters per month (shading) for (a) DJF, (b) MAM, (c) JJA, and (d) SON. The black lines gives percentages of the corresponding precipitation climatology by Xie and Arkin (1996, 1997) with contours of 10%, 20%, 40%, and 60%.

per month. Technically, 6-hourly changes of specific humidity along individual trajectories are evaluated and decreasing values are associated with immediate precipitation at the central point of this 6-hourly trajectory segment (cf. Wernli 1997; Eckhardt et al. 2004). The obtained estimates should be regarded as upper bounds for precipitation, since mixing with drier air and evaporation on the way to the ground are not taken into

account in this analysis. Results for the four seasons are given in Fig. 11, including the corresponding percentages with respect to the long-term precipitation climatology for the years 1979–2002 of Xie and Arkin (1996, 1997). All four seasons show two activity maxima related to the Atlantic and Pacific storm tracks, while values over most parts of Europe, Africa, and Asia are small (Fig. 11). There is a general tendency for a weak

subtropical maximum around 20°N and a larger and more intense maximum at southern midlatitudes (40°–50°N). The former is most likely a reflection of the fact that the extratropical disturbances that instigate TME also trigger precipitation in the subtropical source regions (Kiladis and Weickmann 1992; Kiladis 1998; Funatsu and Waugh 2008). Together with the relatively small variations in total water vapor transport in the latitude band 25°–35°N (Fig. 10), this result implies an uptake of water by evaporation in this region to compensate for the losses through precipitation. The fixation of this maximum to 20°N is presumably to some degree caused by the design of the TME identification algorithm (see section 2). The precipitation signal to the north of 35°N is the actual aim of this work and shall now be discussed in more detail.

The winter season shows a clear signal related to PE transports with a local maximum right over Hawaii and an extended region with more than 20 millimeters per month reaching from the United States and Canadian Pacific coast to beyond 170°W (Fig. 11a). Contributions to climatology exceed 20% in large parts of this region and near Hawaii. This indicates a considerable contribution to precipitation totals, while many case studies have suggested an even more significant contribution to extreme events (see sections 1 and 3). A detailed investigation of this linkage is beyond the scope of this paper and is left for future studies. The Atlantic sector shows a maximum of more than 30 millimeters per month around 40°N, 60°W associated with GS transports and a weaker maximum over the eastern United States (Fig. 11a). Relative contributions are below 20% over the extratropical Atlantic, while values of more than 40% occur in the subtropics. It is interesting to note that the arid belt spanning the Sahara and Arabian Peninsula receives relative contributions of more than 10% associated with both the far end of the Atlantic storm track and occasional local TME trajectories (see, e.g., Fig. 3a). Another unexpected result is the relative contribution of 40% at the very beginning of the Pacific storm track over Southeast Asia.

Spring shows a pronounced eastward shift of activity over the Pacific with a maximum of more than 50 millimeters per month to the west of Japan (Fig. 11b), corresponding to relative contributions of well beyond 20%. In the Atlantic sector the activity maximum shifts to the central United States, reflecting the increase in GP with respect to GS transports discussed earlier. Relative contributions of at least 20% are found along the entire GP track from the Yucatán Peninsula (60%) across the Gulf of Mexico into the midwestern United States (40%). Absolute and relative contributions to European/North African precipitation are largest with maxima over the

Sahara beyond 40%. In JJA the zonal extension of the TME-related precipitation is much smaller than in the other three seasons, reflecting the weaker westerly flow at midlatitudes during this time of year (Fig. 11c). Total values are the highest of all seasons, with TME contributions of more than 70 millimeters per month over Japan and Korea and of more than 50 millimeters per month over the central United States. Relative contributions reach over 60% to the west of Japan and over Texas. The TME-related precipitation during autumn shows an overall similar pattern to spring but with generally weaker absolute and relative contributions (Fig. 11d). Again, there are fairly large relative values over the Sahara in this season.

This analysis shows that TME contributes significantly to climatological precipitation in the subtropics and southern midlatitudes, regionally with more than 60%. Generally speaking, the relative contributions of TME to the extratropical rainfall (Fig. 11) and to the moisture exports across 35°N (Table 1) are of the same order except for regions/seasons with small absolute climatological values such as PE outside of winter. From various case studies (see section 1) and model experiments using water vapor tagging methods (H. Sodemann, Norwegian Institute for Air Research, 2009, personal communication), it seems justified to hypothesize that TME events tend to be involved in heavy rather than low-intensity events, but this is to be verified elsewhere.

7. Summary and conclusions

Tropical moisture exports (TMEs) to the Northern Hemispheric extratropics are an important feature of the general circulation of the atmosphere and link tropical moisture sources with extratropical precipitation and occasionally with explosive cyclogenesis. Based on extensive trajectory computations, an objective 23-year TME climatology has been constructed and analyzed with respect to spatial and temporal variations of TME and their contributions to total moisture transports and precipitation. The employed TME identification routine requires a trajectory origin to the south of 20°N, a circulation to 35°N within seven days or less, and a water vapor flux of at least 100 g kg^{-1} m s^{-1} somewhere to the north of this latitude. In its present form, this method does not quantify the uptake of water vapor along the track. The large number of trajectories above the PBL to the north of 35°N, however, suggests that the impact of ocean evaporation on TME trajectories is most likely relevant in the subtropics only.

Four discrete Northern Hemispheric TME regions with different seasonal behaviors are identified: The "pineapple express" region connects the tropical central

Pacific near the Hawaiian Islands with precipitation near the west coast of North America and is most active in winter. The west Pacific region, in contrast, is most active in summer and to some degree related to the East Asian monsoon and the activity of the mei-yu–baiu front. Because of the large longitudinal and vertical extent of TME in this region, in combination with high water vapor loadings related to the very warm SSTs of the west Pacific and surrounding waters, the total TME during this time of year accounts for a third of the hemispheric TME for the entire year. The narrow Great Plains region connects moisture sources over the Caribbean Sea and the Gulf of Mexico with precipitation in the central United States and also has an activity maximum in the warm season. The Gulf Stream activity maximum reflects water vapor transports from low latitudes into the entrance region of the North Atlantic storm track and has the smallest annual cycle. Precipitation related to this TME mainly affects the open ocean, while Europe and northern Africa are also occasionally reached. All four regions show substantial interannual variability in total TME. El Niño events significantly reduce TME in the pineapple express region and enhance it over the western Atlantic. The North Atlantic Oscillation does not appear to have a significant influence on TME.

On average, TME events are the result of both circulation (i.e., anomalously southerly winds) and moisture anomalies and are characterized by coherent trajectory ensembles over a longitudinally relatively narrow span in the subtropics. Typical lifetimes of such ensembles are several days. On average TME trajectories follow a quasi-horizontal northward track in the subtropics, mostly below 550 hPa, and then ascend northeastward into the midlatitudes. This suggests that many of them could be considered as the far tropical/subtropical inflow into WCBs (Wernli 1997; Eckhardt et al. 2004). It is also noteworthy that in a first one-month statistical study of the frequency of coherent moist ascending airstreams, some of these features originated to the south of 20°N (Wernli and Davies 1997, their Fig. 14). In the extratropics TME trajectories are involved in orographic and storm-track precipitation in both major ocean basins and over East Asia and North America. Relative contributions reach more than 60% to the east of Japan during summer. In addition, there is a smaller contribution of TME situations to precipitation generation in the subtropics, most likely related to the far southward penetration of extratropical upper-level disturbances that instigate poleward moisture transport and at the same time trigger rainfall at low latitudes. As total moisture transports do not decrease strongly up to 35°N, these losses are most likely compensated by water vapor uptake along the track. Contributions of TME to climatological moisture transports across 35°N reach 54% over the west Pacific in summer.

This analysis shows that the bulk of TME is related to the western part of the two big ocean basins, where warm SSTs and southerly flow associated with the western flank of the marine subtropical highs and monsoon circulations favor poleward transports. The associated precipitation falls mainly over the downstream ocean surfaces but also affects surrounding continents, most strongly North America and East Asia. Cases of TME over West Africa like the ones described by Fink and Knippertz (2003) and Knippertz and Martin (2005) are more unusual in a climatological sense but are also reflected in our analysis. The TME climatology presented here, to the best of our knowledge the first of its kind, will serve as a basis for further studies of this important component of the general circulation. The presumably most important aspect is to establish a closer link with high-impact weather events such as heavy precipitation and explosive cyclogenesis. Such an analysis should also include a careful evaluation of null cases, that is, situations with substantial TME but without considerable impacts in the extratropics. Another interesting research path is an investigation of the evolution of vorticity and potential vorticity along TME trajectories (see, e.g., the work of Rodwell and Hoskins 1995). More specifically such a study would address the dynamical question to what degree diabatic processes such as latent heating and friction along the TME trajectories support the northward protrusion of moisture.

REFERENCES

Adams, D. K., and A. C. Comrie, 1997: The North American monsoon. *Bull. Amer. Meteor. Soc.,* **78,** 2197–2213.

Bao, J.-W., S. A. Michelson, P. J. Nieman, F. M. Ralph, and J. M. Wilczak, 2006: Interpretation of enhanced integrated water vapor bands associated with extratropical cyclones: Their formation and connection to tropical moisture. *Mon. Wea. Rev.,* **134,** 1063–1080.

Browning, K. A., 1990: Organization of clouds and precipitation in extratropical cyclones. *Extratropical Cyclones: The Erik H. Palmén Memorial Volume,* C. Newton and E. Holopainen, Eds., Amer. Meteor. Soc., 129–153.

Carlson, T. N., 1980: Airflow through midlatitude cyclones and the comma cloud pattern. *Mon. Wea. Rev.,* **108,** 1498–1509.

Cavazos, T., and D. Rivas, 2004: Variability of extreme precipitation events in Tijuana, Mexico. *Climate Res.,* **25,** 229–243.

Chang, C.-P., and T. N. Krishnamurti, 1987: *Monsoon Meteorology.* Oxford University Press, 560 pp.

Eckhardt, S., A. Stohl, H. Wernli, P. James, C. Forster, and N. Spichtinger, 2004: A 15-year climatology of warm conveyor belts. *J. Climate,* **17,** 218–237.

Fink, A. H., and P. Knippertz, 2003: An extreme precipitation event in southern Morocco in spring 2002 and some hydrological implications. *Weather,* **58,** 377–387.

Funatsu, B. M., and D. W. Waugh, 2008: Connections between potential vorticity intrusions and convection in the eastern tropical Pacific. *J. Atmos. Sci.,* **65,** 987–1002.

Higgins, R. W., J.-K. E. Schemm, W. Shi, and A. Leetma, 2000: Extreme precipitation events in the western United States related to tropical forcing. *J. Climate,* **13,** 793–820.

Huffman, G. J., R. F. Adler, S. Curtis, D. T. Bolvin, and E. J. Nelkin, 2007: Global rainfall analyses at monthly and 3-hr time scales. *Measuring Precipitation from Space: EURAINSAT and the Future,* V. Levizzani, P. Bauer, and F. J. Turk, Eds., Springer Verlag, 291–306.

Iskenderian, H., 1995: A 10-year climatology of Northern Hemisphere tropical cloud plumes and their composite flow patterns. *J. Climate,* **8,** 1630–1637.

Jones, P. D., T. Jónsson, and D. Wheeler, 1997: Extension to the North Atlantic oscillation using early instrumental pressure observations from Gibraltar and south-west Iceland. *Int. J. Climatol.,* **17,** 1433–1450.

Jones, S. C., and Coauthors, 2003: The extratropical transition of tropical cyclones: Forecast challenges, current understanding, and future directions. *Wea. Forecasting,* **18,** 1052–1092.

Kållberg, P., P. Berrisford, B. Hoskins, A. Simmons, S. Uppala, S. Lamy-Thépaut, and R. Hine, 2005: ERA-40 Atlas. ERA-40 Project Report Series 19, ECMWF, 191 pp.

Kiladis, G. N., 1998: Observations of Rossby waves linked to convection over the eastern tropical Pacific. *J. Atmos. Sci.,* **55,** 321–339.

——, and K. M. Weickmann, 1992: Extratropical forcing of tropical Pacific convection during northern winter. *Mon. Wea. Rev.,* **120,** 1924–1938.

Knippertz, P., 2003: Tropical–extratropical interactions causing precipitation in northwest Africa: Statistical analysis and seasonal variations. *Mon. Wea. Rev.,* **131,** 3069–3076.

——, and J. E. Martin, 2005: Tropical plumes and extreme precipitation in subtropical and tropical West Africa. *Quart. J. Roy. Meteor. Soc.,* **131,** 2337–2365.

——, and ——, 2007: A Pacific moisture conveyor belt and its relationship to a significant precipitation event in the semiarid southwestern United States. *Wea. Forecasting,* **22,** 125–144.

——, A. H. Fink, A. Reiner, and P. Speth, 2003: Three late summer/early autumn cases of tropical–extratropical interactions causing precipitation in Northwest Africa. *Mon. Wea. Rev.,* **131,** 116–135.

Mass, C., 2008: *The Weather of the Pacific Northwest.* University of Washington Press, 281 pp.

Matthews, A. J., and G. N. Kiladis, 1999: Interactions between ENSO, transient circulation, and tropical convection over the Pacific. *J. Climate,* **12,** 3062–3086.

McGuirk, J. P., A. H. Thompson, and N. R. Smith, 1987: Moisture bursts over the tropical Pacific Ocean. *Mon. Wea. Rev.,* **115,** 787–798.

Newell, R. E., and Y. Zhu, 1994: Tropospheric rivers: A one-year record and a possible application to ice core data. *Geophys. Res. Lett.,* **21,** 113–116.

——, N. E. Newell, Y. Zhu, and C. Scott, 1992: Tropospheric rivers?—A pilot study. *Geophys. Res. Lett.,* **19,** 2401–2404.

Ninomiya, K., and Y. Shibagaki, 2007: Multi-scale features of the Meiyu–Baiu front and associated precipitation systems. *J. Meteor. Soc. Japan,* **85B,** 103–122.

Pauluis, O., A. Czaja, and R. Korty, 2008: The global atmospheric circulation on moist isentropes. *Science,* **321,** 1075–1078.

Peixoto, J. P., and A. H. Oort, 1992: *Physics of Climate.* American Institute of Physics, 520 pp.

Ralph, F. M., P. J. Nieman, and G. A. Wick, 2004: Satellite and CALJET aircraft observations of atmospheric rivers over the eastern North Pacific Ocean during the winter of 1997/98. *Mon. Wea. Rev.,* **132,** 1721–1745.

Rasmusson, E. M., and K. Mo, 1993: Linkages between 200-mb tropical and extratropical circulation anomalies during the 1986–1989 ENSO cycle. *J. Climate,* **6,** 595–616.

Reed, R. J., M. D. Albright, A. J. Sammons, and P. Undén, 1988: The role of latent heat release in explosive cyclogenesis: Three examples based on ECMWF operational forecasts. *Wea. Forecasting,* **3,** 217–229.

Rodwell, M. J., and B. J. Hoskins, 1995: A model of the Asian summer monsoon. Part II: Cross-equatorial flow and PV behavior. *J. Atmos. Sci.,* **52,** 1341–1356.

Sanders, F., and J. R. Gyakum, 1980: Synoptic-dynamic climatology of the "bomb." *Mon. Wea. Rev.,* **108,** 1589–1606.

Shapiro, M. A., H. Wernli, N. A. Bond, and R. Langland, 2001: The influence of the 1997–99 El Niño Southern Oscillation on extratropical baroclinic life cycles over the eastern North Pacific. *Quart. J. Roy. Meteor. Soc.,* **127,** 331–342.

Stohl, A., C. Forster, and H. Sodemann, 2008: Remote sources of water vapor forming precipitation on the Norwegian west coast at 60°N—A tale of hurricanes and an atmospheric river. *J. Geophys. Res.,* **113,** D05102, doi:10.1029/2007JD009006.

Uppala, S. M., and Coauthors, 2005: The ERA-40 Re-Analysis. *Quart. J. Roy. Meteor. Soc.,* **131,** 2961–3012.

Walker, C. C., and T. Schneider, 2006: Eddy influences on Hadley circulations: Simulations with an idealized GCM. *J. Atmos. Sci.,* **63,** 3333–3350.

Wernli, H., 1997: A Lagrangian-based analysis of extratropical cyclones. II: A detailed case study. *Quart. J. Roy. Meteor. Soc.,* **123,** 1677–1706.

——, and H. C. Davies, 1997: A Lagrangian-based analysis of extratropical cyclones. I: The method and some applications. *Quart. J. Roy. Meteor. Soc.,* **123,** 467–489.

Xie, P., and P. A. Arkin, 1996: Analyses of global monthly precipitation using gauge observations, satellite estimates, and numerical model predictions. *J. Climate,* **9,** 840–858.

——, and ——, 1997: Global precipitation: A 17-year monthly analysis based on gauge observations, satellite estimates, and numerical model outputs. *Bull. Amer. Meteor. Soc.,* **78,** 2539–2558.

Zhu, Y., and R. E. Newell, 1994: Atmospheric rivers and bombs. *Geophys. Res. Lett.,* **21,** 1999–2002.

——, and ——, 1998: A proposed algorithm for moisture fluxes from atmospheric rivers. *Mon. Wea. Rev.,* **126,** 725–735.